TÜBİTAK

Turkish Journal of Zoology

Volume 47 | Number 6 Article 4

11-7-2023

Structural and biological characterization of two freshwater mussel shells (Bivalvia: Unionidae)

HÜLYA ŞEREFLİŞAN

TÜBİTAK

Turkish Journal of Zoology

http://journals.tubitak.gov.tr/zoology/

Research Article

Turk J Zool
(2023) 47: 479-491

doi:10.55730/1300-0179.3149

Structural and biological characterization of two freshwater mussel shells (Bivalvia: Unionidae)

Hülya ŞEREFLİŞAN
Marine Sciences and Technology Faculty, İskenderun Technical University, Hatay, Turkiye

Received: 21.06.2023 • **Accepted/Published Online:** 04.10.2023 • **Final Version:** 07.11.2023

Abstract: The shell of a freshwater mussel (Mollusca: Bivalvia) is a composite biological material that plays an active role in maintaining ecosystem services. Mussel shells have variable structures both within and between species. In this study, the structural and biological characteristics of the shells of *Potomida semirugata* and *Leguminaia wheatleyi* were investigated in order to use freshwater mussel shells as a biological material. Close observation of the microstructure of the shells of the two common freshwater bivalves revealed a variation in construction from the outer periostracum to the inner nacreous layer. In *P. semirugata*, a polygonal arrangement with columnar prisms of different sizes was observed more significantly. In *L. wheatleyi* the prismatic columns are oval and irregularly polygonal. The nacreous layers of *P. semirugata*, in which the individual aragonite layers are horizontally overlapped, are more uniformly distributed. The overlapping of the aragonite sheets in *L. wheatleyi* is more irregular. The presence of calcium carbonate ($CaCO_3$) in the shells was confirmed by the identification of the characteristic carbonate bands at 701.9, 713.5, and 865.8 cm^{-1}. This information was used to classify and distinguish the different layers of the shells, allowing interspecific comparisons and variations in the different layers. The results clearly showed that shell samples were highly biocompatible and nontoxic compared to the control group. This finding suggests that these materials have promising potential for use in various biomedical applications where biocompatibility is a critical factor. The results indicated that the shells of the freshwater bivalves *P. semirugata* and *L. wheatleyi* are biological materials with potential multiple applications for human well-being and environmental quality.

Key words: Calcification, freshwater bivalve, biomineralization, biological material, nacre, scanning electron microscope

1. Introduction

Freshwater mussels have a unique shell structure that is hinged together to protect and support the body (Carter, 1990). Two symmetrical calcareous valves are organomineral composites, and these minerals are generally composed of calcium carbonate ($CaCO_3$) in the form of calcite and/or aragonite. $CaCO_3$ is the component that makes up the majority of bivalve shells, but traces of inorganic elements are also present. Unionid shells are characterized by an outer periostracum, an aragonitic prismatic layer, and an inner nacreous layer (Jackson et al., 1988). Due to their different microstructures, mussel shells vary greatly in shape, size, color, and biomass (Lopes-Lima, 2010). The biomineralization process in bivalves is a unique species-specific architecture (Marin et al., 2012; Marie et al., 2017). Mussel shells, with their extraordinary architecture, have attracted attention as a material that can be used in many fields. To this end, many scientists have studied the definition of the microstructures of freshwater mussel shells (Hedegaard, 1990; Machado et al. 1991; Hedegaard, 1997; Moura et al. 2000; Lopes-Lima, 2010; Chakraborty et al., 2020). Indeed, mussels play a major role in natural habitats, both alive and with their perfectly formed shells (Binelli et al., 2014). While freshwater mussel shells are used as seeds in oyster farming, their shells are mostly waste (Anthony and Downing 2001; Haag 2012). Waste shells are a highly valuable resource that is applicable to be used for many purposes (Yao et al., 2014) due to their high $CaCO_3$ content. Thus far, they have been successfully used for the mining industry (i.e. for sulphate reduction), wastewater treatment, reinforced composite production, environmental remediation (i.e. metal and paint removal, treatment of eutrophic waters), agriculture (i.e. soil improvement), bone regeneration, and cement replacement (Lee et al., 2010; Álvarez et al.2012; Hamester et al., 2012; González-Chang et al., 2017; Delali et al., 2019). Mussel shells, which preserve the ecology and have a high marketing value, are a true aquaculture biomaterial of significant value (Chakraborty et al., 2020). The characterization of mussel shells, which

* Correspondence: hulya.sereflisan@iste.edu.tr

are so widely used, is of great importance. The discovery of the cross-layered aragonite structure has contributed to the preference of shells as biological materials (Meyers et al. 2008). The genus *Potomida* (Bivalvia, Unionida), which has a long history of taxonomic revisions, has a circum-Mediterranean distribution and *P. semirugata* populations have suffered dramatic declines in most rivers (Lake Gölbaşı) in southern Türkiye (Froufe et al., 2016). *L. wheatleyi*, the subfamily Gonideinae, is present in Gölbaşı Lake in southeastern Türkiye (Tomilova et al., 2020; Lopes-Lima et al., 2021). *P. semirugata* and *L. wheatleyi* are freshwater bivalves commonly found in Lake Gölbaşı. These species, whose habitats are muddy and sandy, migrate to deeper waters when the water temperature drops and live by burying themselves in sediments. In general, they do not prefer areas with aquatic plants as their habitat. They live by burying themselves in the sediment at a depth of 30–40 cm in warm, shallow, stagnant waters. Gölbaşı Lake is an important lake where many people depend on fishing for their livelihood. However, *P. semirugata* and *L. wheatleyi* are not sought after for their meat and shells, and their shells are abundant on the lake shore and in the substrate (Şereflişan, 2003). In the present study, the physical characteristics, chemical composition, and various biological properties of freshwater mussel shells were investigated to substantiate their potential as a useful biological material. The size (length and height), shape, and microstructure of the shells were studied to understand their physical characteristics. The chemical and microstructural composition of the shells was analyzed to determine their mineral content and present organic compounds. Various biological properties of the mussel shells were also investigated, such as their biocompatibility, hemocompatibility properties, and potential as a source of biomaterials.

2. Materials and methods

2.1. Study area

The sample collection was carried out at Gölbaşı Lake, located in the Hatay Province of southern Türkiye. Gölbaşı Lake (36°29′E, 36°30′N) covers an area of approximately 400 ha (4,000,000 m^2) (Figure 1). It is a natural lake that is fed by groundwater at various places. The sampled lake has a very high fishing pressure, and it is considered to be an important habitat for *P. semirugata* and *L. wheatleyi* (Şereflişan, 2003).

2.2. Preparation of the samples

Freshwater mussels *P. semirugata* and *L. wheatleyi* (Figure 2) were collected from Gölbaşı Lake in June 2022. Their shells were rinsed with deionized water. Then, the shell length and height of the freshwater mussel species were measured with digital calipers with 0.05-mm accuracy. The shell length, height, habitats, and distributions (Lopes-Lima et al. 2021) of the studied species are presented in the Table.

2.3. Scanning electron microscope (SEM) and energy-dispersive X-ray spectroscopy (EDS) analyses

The surfaces and structures of the *P. semirugata* and *L. wheatleyi* shells were visualized via SEM. The specimens

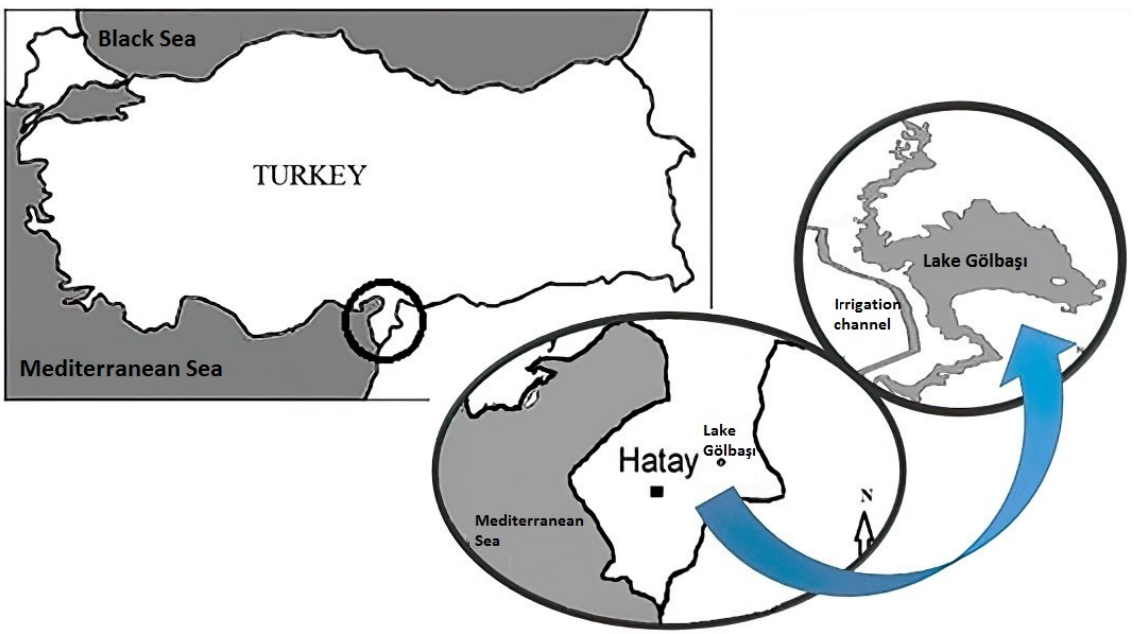

Figure 1. Study area.

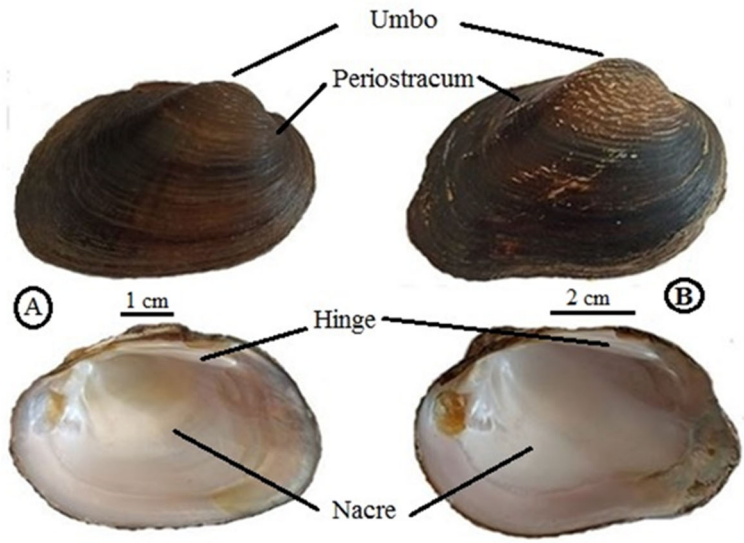

Figure 2. (**A**) *Potomida semirugata* and (**B**) *Leguminaia wheatleyi*.

Table. Morphological characteristics (length in centimeters and weight in grams), and distribution of 2 freshwater mussel shells.

Species	n	Length	Height	Distribution
P. semirugata	20	6.7 ± 0.38	2.9 ± 0.50	Northwestern Türkiye, Eastern Mediterranean
L. wheatleyi	20	8.1.3 ± 0.33	2.8 ± 0.32	Türkiye, Eastern Mediterranean

were mounted on the stubs by gold-plating using a Polaron SC7620 apparatus in a sputter coater before use in the SEM. An electron acceleration potential of 15 kV was used for the microscopic observations. Photographs were taken in a SEM (JEOL JSM-638OLA; Akishima, Tokyo, Japan) at the required magnification. Chemical composition and elemental characterization of the freshwater mussel shells were carried out using the EDS attached to the SEM.

2.4. Fourier-transform infrared (FTIR) spectroscopy analysis

The study was carried out by first mixing 100 mg of KBr with 1% dried shell dust (separately for *P. semirugata* and *L. wheatleyi*). The mixture was then ground to form shell dust KBr pellets for the FTIR spectrum analysis. The infrared spectrum attributable to the shell dust was obtained using an FTIR spectrometer (Jasco FT/IR-6300 type A; serial no. A014461024). For both shell species, the spectra were collected at a resolution of 4 cm $^{-}$1 with a scan speed of 2 mm/s in the range of 500 to 3500 wavenumbers (cm $^{-}$1) (Hossain and Aditya, 2013).

2.5. Hemocompatibility test

To assess the hemocompatibility of the freshwater mussel (*P. semirugata* and *L. wheatleyi*) shell powders, their hemolytic activity percentages were determined using the modified method described elsewhere (Wang et al., 2012; Alexandre et al., 2014). Briefly, fresh blood was collected from a healthy sheep at a slaughterhouse and then stabilized with dipotassium ethylenediaminetetraacetic acid (1.5 mg L^{-1}). To obtain healthy red blood cells (HRBCs) for the hemolysis assay, the fresh blood was centrifuged immediately after collection (5000 rpm for 3 min), washed 3 times, and then diluted 10-fold with sterile phosphate-buffered saline (PBS) solution. Then, 2 mL of the diluted HRBCs suspension was transferred to a 5-mL sample vial containing 25 mg of *P. semirugata* and *L. wheatleyi* freshwater mussel shell powder, respectively. Two further sample vials containing 0.4 mL of the diluted erythrocytes and 1.6 mL of sterile distilled water or PBS solution were used as the positive and negative controls, respectively. All of the blood mixtures were then incubated at 37 °C for 2 h, followed by centrifugation (10,000 rpm, 1 min), and the absorbance of the supernatants related to hemoglobin was recorded at 541 nm using a Spectro star Nano (BMG Labtech, Ortenberg, Germany) equipped with a BMG Labtech ultrafast UV/Vis spectrometer. Hemolytic activity was confirmed twice for each sample

and the average of two independent experiments was used to calculate the percentage of hemolytic activity. The percentage of hemolytic activity was calculated using the equation below (1):

$$HA\ (\%) = \frac{OD_S - OD_{NC}}{OD_{PC} - OD_{NC}}\ x\ 100. \quad (1)$$

Here, OD_S is the absorbance of the tested sample, OD_{NC} is the absorbance of the negative control, and OD_{PC} is the absorbance of the positive control.

2.6. Evaluation of the blood clotting property

To assess the blood clotting index (BCI) of the freshwater mussel (*P. semirugata* and *L. wheatleyi*) shell powders, the method described by Patil et al. (2018) was used with some modifications. For the analysis, sheep blood was collected at the abattoir in a anticoagulant tube and used immediately. The study was briefly performed as follows: Sponge samples were placed in the center of polypropylene petri plates and 100 µL of blood was applied to the surface of the samples. Immediately afterwards, 10 µL of 0.2M $CaCl_2$ solution was dropped onto the surface and the samples were incubated at 37 °C for 20 min. At the end of the incubation period, 5 mL of sterile distilled water was gently added without breaking up the formed clot. In the next step, the blood-water mixture in the plates was collected and transferred to a polypropylene test tube. After centrifugation at 10,000 rpm, the supernatants were transferred to clean tubes and incubated at 37 °C for 1 h. At the end of the incubation period, the optical density of the samples was recorded at 540 nm using a Spectro star Nano (BMG Labtech) equipped with a BMG Labtech ultra-fast UV/Vis spectrometer. For the optical density measurements, sterile distilled water was used as the target and 5 mL of sterile distilled water with 100 µL of the blood mixture (which was subjected to all of the analysis steps) was used as the positive control. The clotting capacity was confirmed twice for each sample and the average of 2 independent experiments was used to calculate the BCI (%). The BCI was calculated according to the equation of Wang et al. (2012):

$$BCI\ (\%) = \frac{OD_S}{OD_{Pc}}\ x\ 100 \quad (2)$$

Here, OD_S is the absorbance of the tested sample and OD_{PC} is the absorbance of the positive control.

2.7. In vitro biocompatibility studies

The in vitro cytotoxicity of the *P. semirugata* and *L. wheatleyi* freshwater mussel shell powders was evaluated using the ISO 10993-5 standard test method. The antiproliferative activities of the samples were measured using the 2, 3-bis-(2-methoxy-4-nitro-5-sulfophenyl)-2H-tetrazolium-5-carboxanilide (XTT reagent) colorimetric assay. L929 mouse fibroblast cells were selected as a model cell line to determine the cytotoxicity of the shell powders for the cytocompatibility assay. The cells were cultured in Dulbecco's modified eagle medium (DMEM) supplemented with 1% (v/v) of a preprepared solution of penicillin (100 U/mL), streptomycin (100 U/mL), and 10% (v/v) fetal bovine serum (FBS) and incubated for 24 h at 37 °C with humidity above 90% in an atmosphere of 5% CO_2. They were seeded at a density of $1 \times 10\ \wedge$ (4) cells/well on a 96-well microplate and incubated at 37 °C for 48 h. After incubation, the cells were treated with different concentrations of compounds (2, 3, 5, and 10 µL) and incubated in an incubator at 37 °C with 5% CO_2 for 48 h. After incubation, the culture medium was discarded, and the wells were rinsed 3 times with PBS. Then, 200 µL of DMEM containing 50 µL of 5 mg/mL XTT reagent was added to each well and incubated for 4 h. The absorbance of the solution was measured spectrophotometrically using a Thermo Scientific Multiskan FC Microplate Photometer reader (Thermo Fisher Scientific Inc., Waltham, MA, USA) at a wavelength of 450 nm. The experiment was repeated in triplicate (Yang et al., 2017; Kucharczyk et al., 2019; Öksüz et al., 2021).

2.8. Statistical analysis

The collected data were presented as the mean ± standard deviation of the mean SD based on at least 6 independent measurements. Data were statistically analyzed using 1-way analysis of variance (ANOVA) followed by the Dunnett and Tukey tests, and significance was achieved at $^*p \leq 0.05$ using Origin Pro 9.0 software (OriginLab Co., Northampton, USA).

3. Results

3.1. Microstructure observation and characterization with the SEM

The protein-containing sclerotized periostracum layer of the shells of both mussels was very prominent (Figures 3A and 3B). Apparently, the outer surface of the periostracum of the shell of *P. semirugata* and *L. wheatleyi* did not consist of radial, oblique ridges. The prismatic layer showed a typical polygonal arrangement, as shown in the magnified image in Figures 4A and 4B. The nacreous layer of the shells of (A) *P. semirugata* and (B) *L. wheatleyi* is shown in the magnified image in Figures 5A and 5B. The internal shell structure of the 2 bivalves differed in terms of the nacre (Figures 6A and 6B). The shell of *L. wheatleyi* showed an irregular crystalline structure in the nacreous layer (Figure 6B). The lateral view of the prismatic layer shows the columnar convergent prisms of (A) *P. semirugata* and (B) *L. wheatleyi* (Figures 7A and 7B). These columns grow within organic membrane structures. While the columnar prismatic structure of *P. semirugata* (Figure 7A)

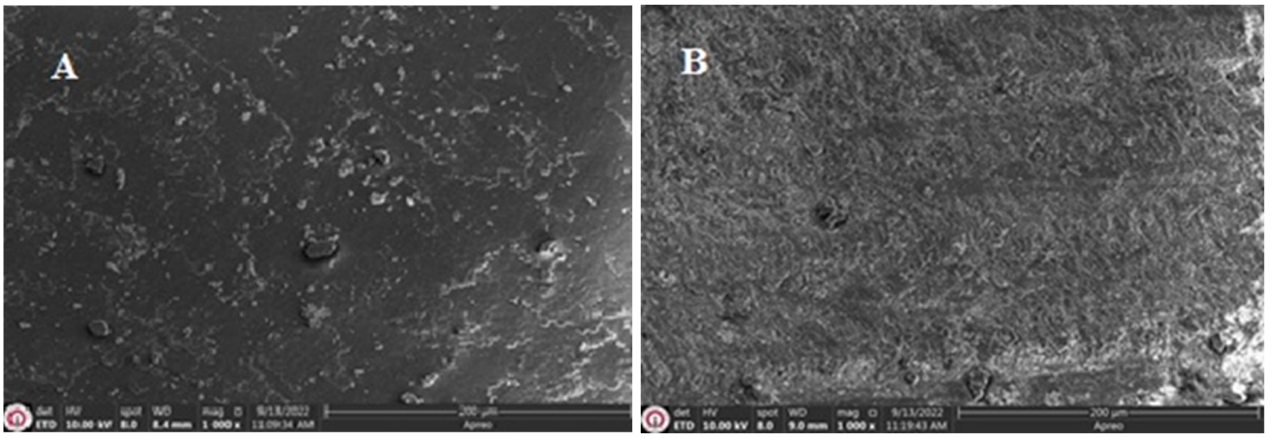

Figure 3. The growth front of the outer surface of each shell of (**A**) *P. semirugata* and (**B**) *L. wheatleyi*.

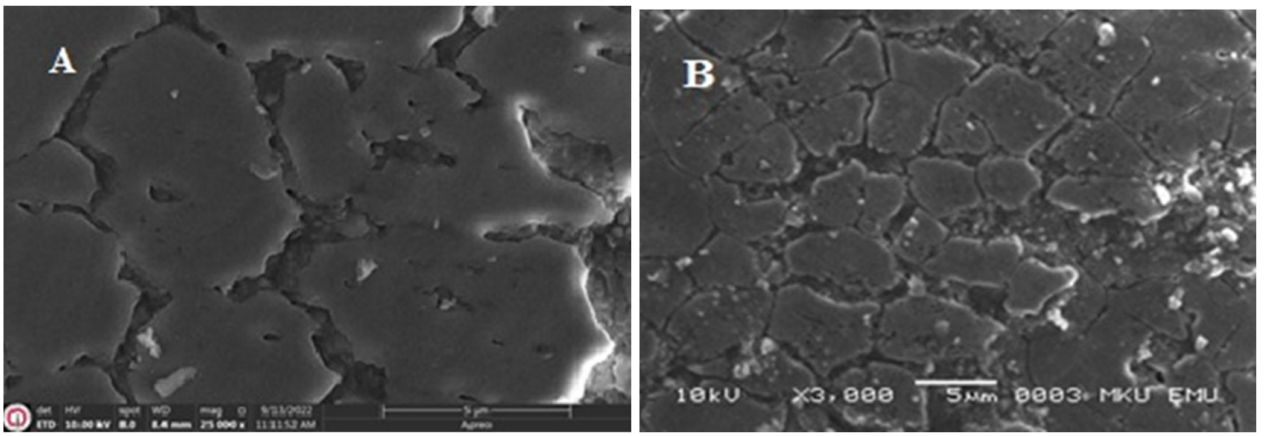

Figure 4. The periostracum on the outer surface of each shell of (**A**) *P. semirugata* and (**B**) *L. wheatleyi.*

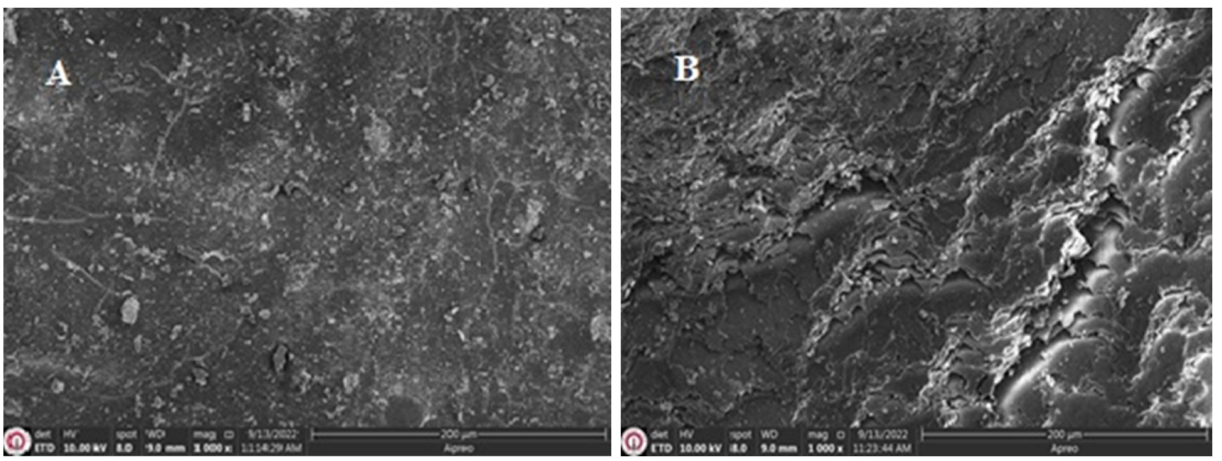

Figure 5. SEM image of the nacreous layer of the shells of (**A**) *P. semirugata* and (**B**) *L. wheatleyi*.

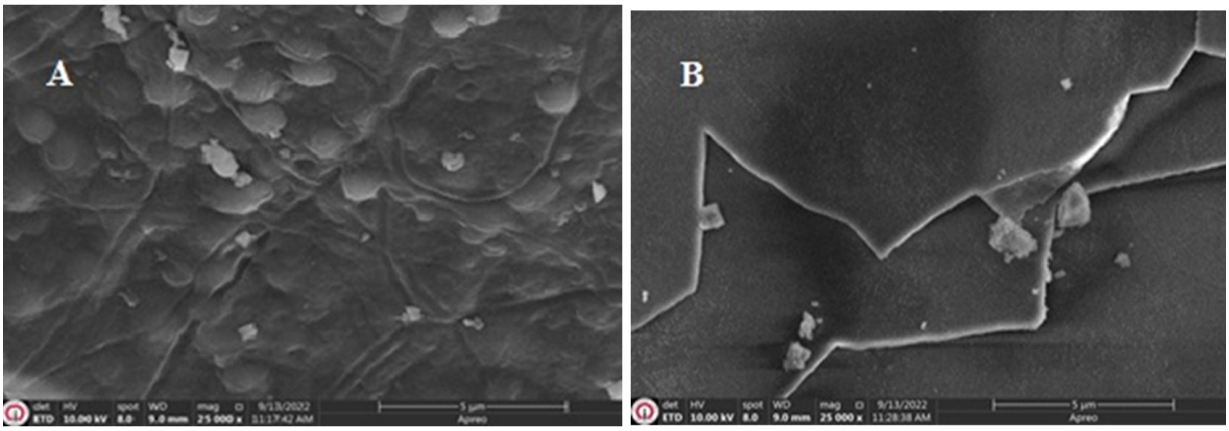

Figure 6. The growth front of the nacre of (**A**) *P. semirugata* and (**B**) *L. wheatleyi*.

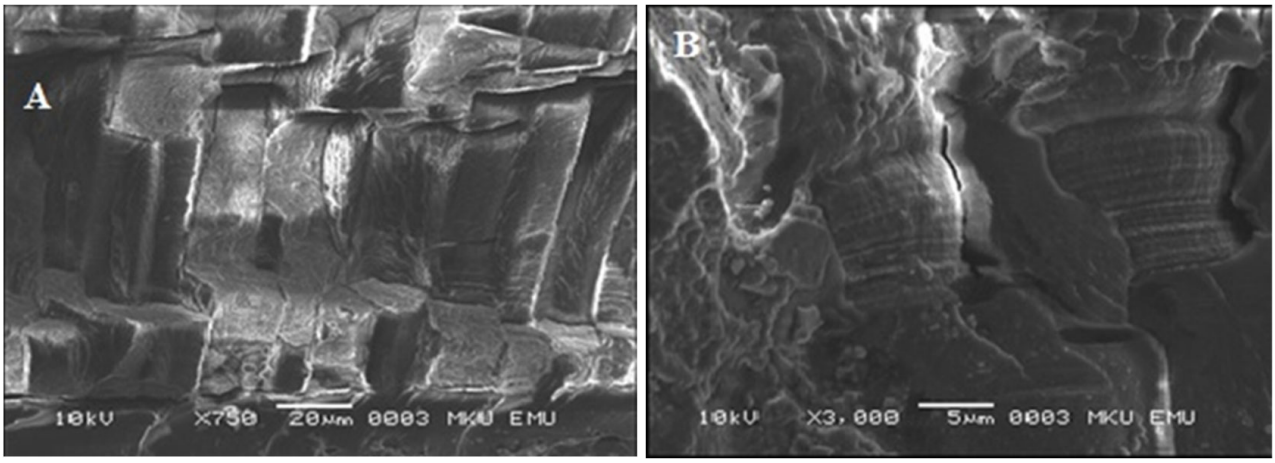

Figure 7. Lateral view of the prismatic layer showing the columnar convergent prisms of (**A**) *P. semirugata* and (**B**) *L. wheatleyi*.

was angular, that of *L. wheatleyi* (Figure 7B) appeared to be more rounded. The horizontally overlapping individual aragonite sheets of *P. semirugata* appeared to be more regular than those of *L. wheatleyi* (Figure 8).

3.2. EDS analysis

Figures 9A and 9B show the SEM images and EDS data of the periostracum and nacreous layers in the *L. wheatleyi* shells, respectively. The semiquantitative chemical composition revealed the presence of Ca, Na, Mg, C, and O. In the nacreous layer of *L. wheatleyi*, the chemical composition of the elements ranged from 12.33 to 12.92 atom% for C, 65.63 to 66.49 atom% for O, 0.14 to 0.2 atom% for Na, 0.07 to 0.09 atom% for Mg, 0.06 to 0.08 atom% for Si, 20.06 to 22.6 atom% for Ca, 0.15 to 0.87 atom% for Zr, and 0.57 to 0.75 atom% for Pt (Figure 9B). The chemical composition of the elements in the periostracum layer of *L. wheatleyi* ranged from 7.28 to 12.85 atom% for C, (52.14 to 67.07 atom%) for O, (0.11 to 0.18 atom%) for Na, (0.09 to 0. 11 atom%) for Al, (19.3 to 39.35 atom%) for Ca, (0.03 to 0.15 atom %) for Zr, (0.49 to 1.12 atom%) for Pt, and (0.06 to 0.07 atom%) for S (Figure 9A).

Figures 10A and 10B show the SEM-EDS images and EDS data of the periostracum and nacreous layers of the *P. semirugata* shells, respectively. The semiquantitative chemical composition showed that Ca, Na, Mg, C and O were the main elements. In the nacre layer of *P. semirugata*, the chemical composition of elements ranged from 53.04 to 65.80 atom% for C, 29.30 to 38.53 atom% for O, 0.16 to 0.27 atom% for Na, 0.06 to 0.13 atom% for Mg, 0.78 to 1.59 atom% for S, and 1.52 to 4.48 atom% for Ca. The chemical composition of the elements in the periostracum layer of *P. semirugata* ranged from 7.28 to 12.85 atom% for C, 52.14 to 67.07 atom% for O, 0.11 to 0.18 atom% for NA, 0.09 to 0.11 atom% for Al, 0.06 to 0.07 atom% for S, and 19.30 to 39.35 atom% for Ca.

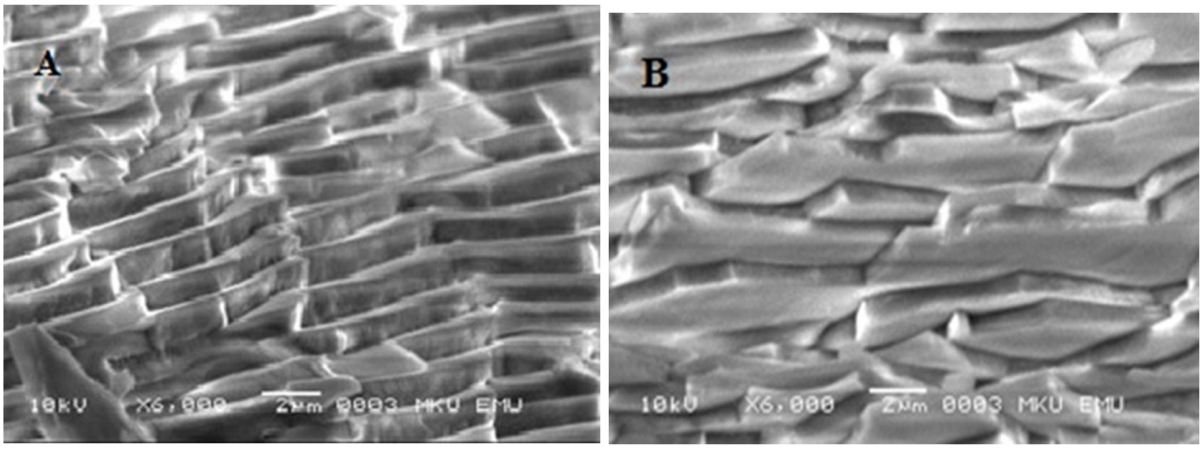

Figure 8. View of the nacre layer of (**A**) *P. semirugata* and (**B**) *L. wheatleyi*, where the individual aragonite layers are horizontally overlapping.

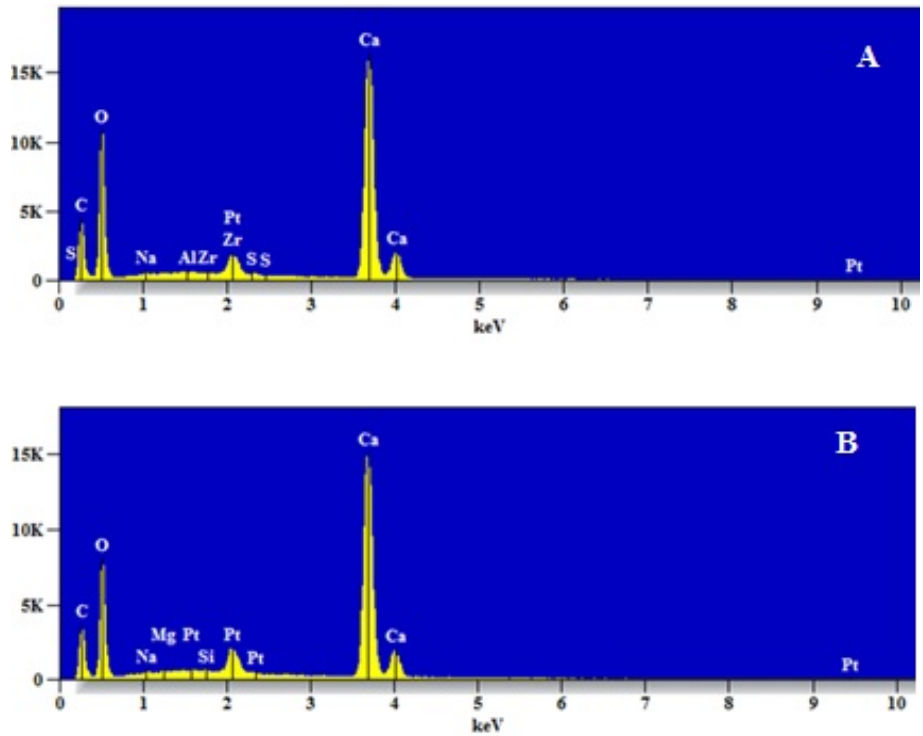

Figure 9. SEM-EDS of the different surfaces of the *L. wheatleyi* shells: (**A**) periostracum layer and (**B**) nacreous layer.

3.3. FTIR analysis

In this experimental study, the functional groups present in the collected mussel shells were analyzed through FTIR spectroscopy. The analysis of the FTIR spectra revealed important information about the functional groups present in the collected mussel shells. Figure 11 shows the FTIR spectra of the two mussel shells, which showed similar characteristics. The peak at 2933.76 cm^{-1} appeared due to the CH_2 stretching bonds of the aliphatic chains. The spectral peak at 2362.54 cm^{-1} was identified as the stretching vibration of COO^- functional groups. The FTIR spectrum showed organic bands of lower intensity; the band at 1786.52 cm^{-1} was attributed to the carboxylate (carbonyl) groups of the acidic proteins in the organic matrix. Four

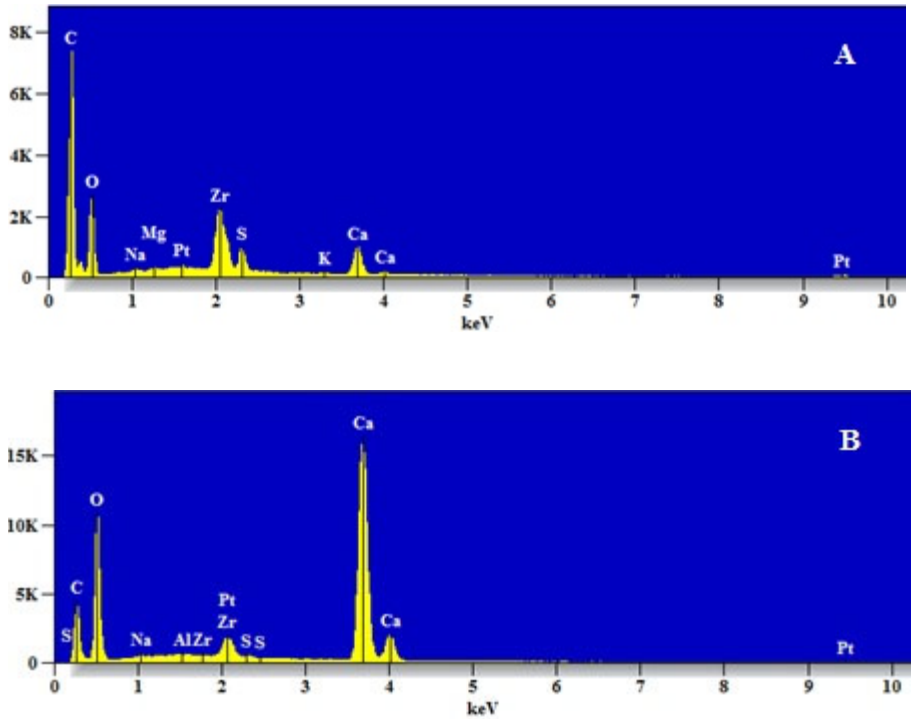

Figure 10 SEM-EDS of the different surfaces of the *P. semirugata* shells: (**A**) periostracum layer and (**B**) nacreous layer.

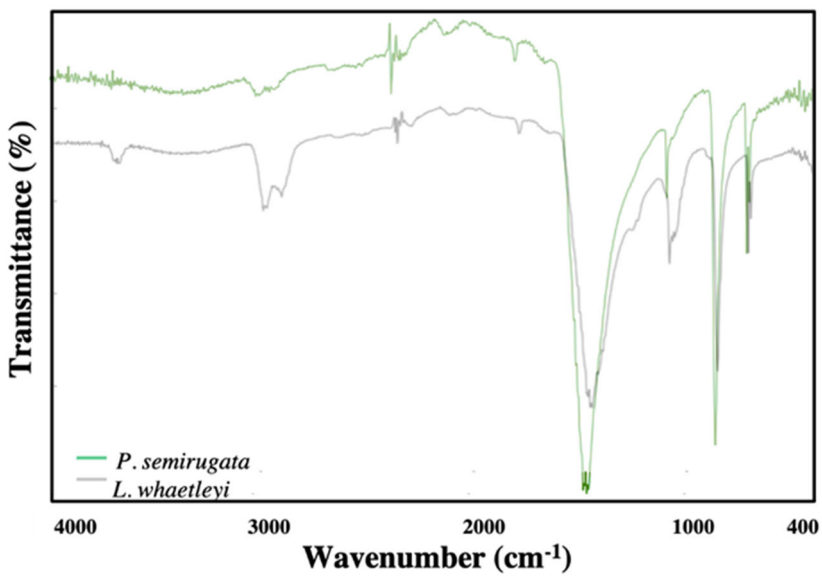

Figure 11. FTIR spectra of the shells of *P. semirugata* and *L. wheatleyi*.

bands characteristic of aragonite, corresponding to the CO_2^{-3} ions, were identified: ν3 at 1467.32 cm^{-1}, ν1 at 1081.43 cm^{-1}, ν2 at 863.39 cm^{-1}, and ν4 at 702.31–713.73 cm^{-1} (Figure 11). The ν4 band corresponded to the planar bending mode of the carbonate vibration and the ν1 band to the symmetric stretching mode.

Moreover, the characteristic carbonate ν4 bands of the aragonite were at 713.73 and 702.31 cm^{-1} and the characteristic carbonate ν2 band of the aragonite was at 863.39 cm^{-1}, indicating the availability of the aragonite form of $CaCO_3$ that is seen in the shell powders of snails (Anjaneyulu et al., 2015; Hossain et al., 2015).

3.4. Hemostatic characterization

The results of the test, including the hemolytic activity (%) and BCI (%), are shown in Figure 12. Fresh blood was used for the test, and the hemolysis rates were 1.97% and 2.07% for the *P. semirugata* and *L. wheatleyi* shells, respectively (Figure 12A). These results showed that the hemolysis rates slightly exhibited the same trend between the mussel shell groups (Figure 12A).

The BCI results were different between the *P. semirugata* and *L. wheatleyi* shells. The shells of *P. semirugata* had a lower BCI value. The shells of *L. wheatleyi* had a higher BCI for clot formation (Figure 12B).

3.5. In vitro biocompatibility studies

The aim of this study was to evaluate the effect of different concentrations of *P. semirugata* and *L. wheatleyi* shell extracts on the proliferation of L929 mouse fibroblast cells using the XTT assay. The XTT assay measured cell viability as a percentage of the viability observed in the mussel shell samples. Figure 13 shows the cell viability plot using the XTT assay and it was observed that all of the groups supported cell proliferation. The results clearly demonstrated that both of the shell samples were highly biocompatible and nontoxic when compared to the control group.

4. Discussion

The chemical composition of the mussel shells, dominated by $CaCO_3$, indicates that they are a source of CO_2, and are therefore important in the carbon cycle (Chakraborty et al., 2020). It involves the calcification of the shell, and the formation of an organic matrix of soluble and insoluble compounds. The presence of $CaCO_3$ is essential for this process (Moura et al. 2000). The bioformed crystals of the shell were quite different in size and shape from those of their nonbiological counterparts (Lopes-Lima et al., 2010). Although the mechanism of biomineralization in molluscs is influenced by environmental factors (such as the physicochemical parameters of the water), it is essentially a cellular process (Moura et al. 2000). Close observation of the microstructure of the shells of two common freshwater bivalves, *P. semirugata* and *L. wheatleyi*, revealed a variation in their construction from the outer periostracum to the inner nacreous layer. In *P. semirugata*, a polygonal arrangement with columnar prisms of different sizes combined was observed to be more pronounced. In *L. wheatleyi* the prismatic columns are oval and irregularly polygonal. The length and orientation of these fibers play an important role in the growth and remodeling of the shell (Dauphin et al., 2018). The nacreous layers of *P. semirugata*, where the individual aragonite sheets are horizontally overlapped, were more evenly arranged. Overlapping of the aragonite layers was more irregular in *L. wheatleyi*.

The analysis of the FTIR spectra revealed important information about the functional groups present in the collected mussel shells. As shown in Figure 2, the peak at about 2933.76 $cm^{-}1$ was attributed to the C-H stretching vibration, indicating the presence of methyl and methylene groups in the shells. The spectral peak at 2362.54 $cm^{-}1$ was identified as the stretching vibration of COO^{-} functional groups. In addition, the band at 1467.32 cm^{-1} corresponded to the C=C bond, which is indicative of unsaturated hydrocarbons. The peak at 1081.43 $cm^{-}1$ was due to C-O stretching, suggesting the presence of proteins in the shell matrix (Marie et al., 2010). The presence of $CaCO_3$ in the mussel shells was confirmed by the identification of the characteristic carbonate bands at 702.31, 713.73, and 863.39 cm^{-1}. This information was used to classify

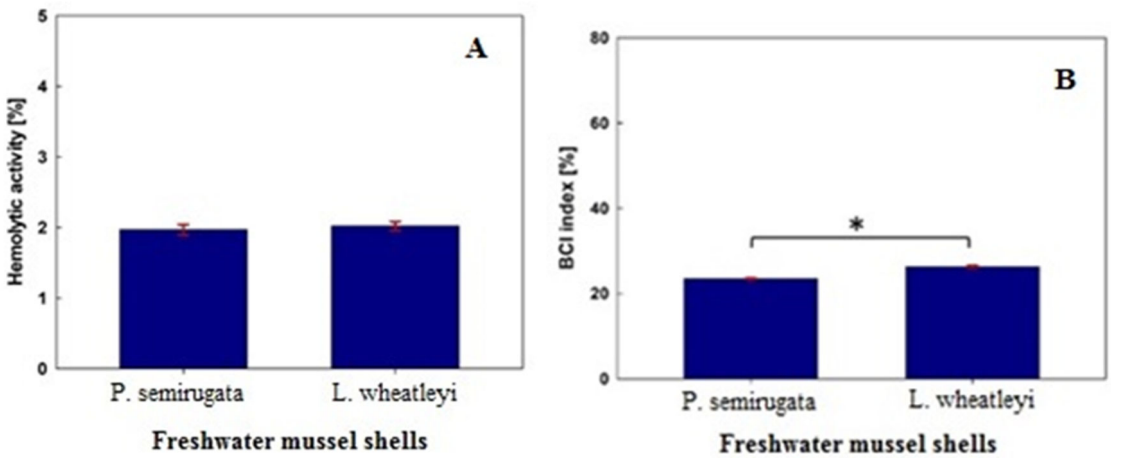

Figure 12. (**A**) Hemolytic activity (%) of the freshwater mussel shell powder. (**B**) BCI (%) of the freshwater mussel shell powder. *Significant differences for all pairwise analyses at $p < 0.05$.

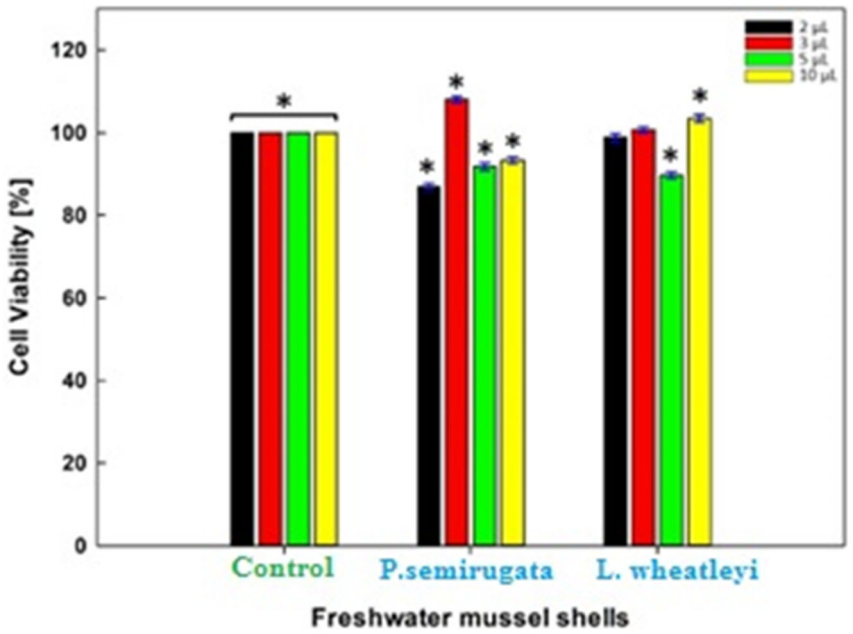

Figure 13. Cell viability (%) of the freshwater mussel shell powder. *Significant differences compared to the control at $p < 0.05$.

and distinguish the different layers of the shells, allowing interspecific comparisons and the study of variations in the different layers. As a result of this analysis, it was possible to identify the different layers of the shell, including the outer periostracum, the middle prismatic layer, and the inner nacreous layer. The outer periostracum is the outermost layer of the shell and consists of organic compounds such as chitin and proteins. The middle prismatic layer consists of densely packed $CaCO_3$ crystals, and the inner nacreous layer consists of $CaCO_3$ in a crystalline form arranged in a specific pattern (Sudo et al., 1997; Lopes-Lima et al., 2010; Carter et al., 2012; Hossain et al., 2015; Agbaje et al., 2017). By distinguishing between the different layers of the shell and examining variation within and between species, a more comprehensive understanding of shell morphology and composition can be obtained. This information can be used to further explore the potential applications of mussel shells in fields such as materials science, biotechnology, and environmental remediation (Carter, 1990).

The results of the test, including the hemolytic activity (%) and coagulation index (%), are shown in Figure 12. Fresh blood was used for the test and the hemolysis rates were 1.97% and 2.07% for the *P. semirugata* and *L. wheatleyi* groups, respectively (Figure 12A). These results showed that the hemolysis rates exhibited slightly the same trend between the shell groups. The number of erythrocytes bound to nanoparticles and the energy of the cell membranes to encapsulate nanoparticles are two factors affecting hemolysis, and both are affected by the external surface area of materials (Yannan et al., 2011). The hemolytic activity of various materials used in healthcare is typically determined and classified according to the American Society for Testing and Materials (ASTM) standards. According to the ASTM F756-00 and ISO 10 993-51, a sample is considered nonhemolytic if the hemolytic index range is less than 2%, mildly hemolytic if it is between 2% and 5%, and hemolytic if it is greater than 5%. In light of the ASTM standards, the hemolysis rates obtained from the mussel shell samples indicated that they are nonhemolytic (Bohorquez-Moreno et al., 2023). Therefore, these results revealed that the studied shells can be used in medical sector applications.

To understand the results of the BCI, it is essential to understand the blood clotting assay, which evaluates the antithrombogenic properties of various biomaterials in contact with whole blood by measuring the amount of free hemoglobin in the medium. Calcium ions play a crucial role in the coagulation reactions that lead to clot formation, making it a critical element of the test (Jang et al., 2010). The BCI results for the *P. semirugata* and *L. wheatleyi* groups were related to their ability to absorb calcium ions. The capacity of the *P. semirugata* shell to absorb calcium ions was limited due to its structural characteristics, resulting in a lower BCI value. On the other hand, the *L. wheatleyi* group had a higher BCI value. This demonstrated that it has a higher tendency toward clot formation since it can

absorb calcium ions more effectively (Singh et al., 2019). The aim of the study was to evaluate the effect of different concentrations of *P. semirugata*, *L. wheatleyi* shell extracts on the proliferation of L929 mouse fibroblast cells using the XTT assay. The XTT assay measured the cell viability as a percentage of the viability observed in the mussel shell samples. Figure 3 shows the cell viability plot using the XTT assay, wherein it can be seen that all of the groups supported cell proliferation with cell viability values above approximately 85%. It was also noted that none of the materials were cytotoxic in the experimental study, as reported in the literature (Latire et al., 2017; El-Bassyouni et al., 2020). Figure 10 shows a significant difference in cell activity for the *P. semirugata* group (107.6 ± 0.8, 3 µL) and the *L. wheatleyi* group (103.4 ± 0.6, 10 µL), indicating their potential to support cell growth. Indeed, mollusc shells contain numerous macromolecules, including soluble proteins, glycoproteins, hydrophobic proteins, chitin, soluble polysaccharides, and lipids (Lowenstam and Weiner 1989; Bédouet et al. 2001; Marie et al. 2011; Marin et al. 2012). *Mytilus edulis* and *Crassostrea gigas* shell extracts have been reported to support cell proliferation, and it has been suggested that shell proteins may play an inducing role in such a finding (Latire et al., 2017). Similarly, a study of the effect of the pearl mussel *Hyriopsis cumingii* Lea on the proliferation of osteoblastic lineage cells showed an increase in the proliferation of these cells (Shen et al. 2006). Although a slight decrease in cell viability was observed in the *P. semirugata* (91.62 ± 0.8, 5 µL) and *L. wheatleyi* (89.25 ± 0.6, 5 µL) groups, the results clearly demonstrated that both shell samples were highly biocompatible and nontoxic compared to the control group. This finding suggests that the materials have promising potential for use in various biomedical applications where biocompatibility is a critical factor. Furthermore, it is important to note that cell viability assays, such as the XTT assay used in this study, are essential tools for assessing the compatibility of new biomaterials and evaluating their effects on cell behavior. The results of this study are consistent with previous studies (Ismail et al., 2021; Zhang et al., 2022) that have demonstrated the excellent biocompatibility of mussel shells and their potential use in various biomedical applications.

5. Conclusion

In this study, the structural and biological characterization properties of the shells of *P. semirugata* and *L. wheatleyi* were investigated from the perspective of using freshwater mussel shells as biological material. Close observation of the microstructure of the shells of the two freshwater mussels revealed a variation in construction from the outer periostracum to the inner nacreous layer. In *P. semirugata*, a polygonal arrangement with columnar prisms of different sizes combined was observed to be more pronounced. In *L. wheatleyi* the prismatic columns are oval and irregularly polygonal. The presence of $CaCO_3$ in the mussel shells was confirmed by the identification of the characteristic carbonate bands at 701.9, 713.5, and 865.8 cm^{-1}. The results clearly demonstrated that both shell samples were highly biocompatible and nontoxic when compared to the control group. The work presented herein shows that the materials have promising potential for use in various biomedical applications where biocompatibility is a critical factor.

Ethical approval

Ethical approval was not needed for this study, as the study dealt with invertebrate organisms.

Acknowledgment

The author thanks Kerim Emre ÖKSÜZ and Erkan UĞURLU for their help with the fieldwork and their comments to improve the manuscript. Thanks are also extended to Ece KILIÇ for the English corrections of the manuscript.

References

Agbaje OBA, Wirth R, Morales LFG, Shirai K, Kosnik M et al. (2017). Architecture of crossed-lamellar bivalve shells: the southern giant clam (*Tridacna derasa*, Röding, 1798). Royal Society Open Science 4 (9): 170622. https://doi.org/10.1098/rsos.170622

Alexandre N, Ribeiro J, Gärtner A, Pereira T, Amorim et al. (2014). Biocompatibility and hemocompatibility of polyvinyl alcohol hydrogel used for vascular grafting - in vitro and in vivo studies. Journal of Biomedical Materials Research Part A 102 (12): 4262-4275. https://doi.org/10.1002/jbm.a.35098

Álvarez E, Fernández-Sanjurjo MJ, Seco N, Núñez A (2012). Use of mussel shells as a soil amendment: effects on bulk and rhizosphere soil and pasture production. Pedosphere 22 (2): 152-164. https://doi.org/10.1016/S1002-0160(12)60002-2

Anjaneyulu U, Pattanayak DK, Vijayalakshmi U (2015). Snail shell derived natural hydroxyapatite: effects. Materials and Manufacturing Processes, 0: 1–11. http://dx.doi.org/10.1080/10426914.2015.1070415

Anthony JL, Downing JA (2001). Exploitation trajectory of a declining fauna: a century of freshwater mussel fisheries in North America. Canadian Journal of Fisheries and Aquatic Sciences 58: 2071–2090. https://doi.org/10.1139/F01-130

Bédouet L, Schuller MJ, Marin F, Milet C, Lopez E et al. (2001). Soluble proteins of the nacre of the giant oyster Pinctada maxima and of the abalone *Haliotis tuberculata*: extraction and partial analysis of nacre proteins. Comparative Biochemistry and Physiology Part B: Biochemistry and Molecular Biology 128 (3): 389-400. https://doi.org/10.1016/S1096-4959(00)00337-7.

Binelli A, Magni S, Soave C, Marazzi F, Zuccato E et al. (2014). The biofiltration process by the bivalve *D. polymorpha* for the removal of some pharmaceuticals and drugs of abuse from civil wastewaters. Ecological Engineering 71: 710-721. https://doi.org/10.1016/j.ecoleng.2014.08.004.

Bohorquez-Moreno CD, Öksüz KE, Dincer E (2023). Porous polymer scaffolds derived from bioresources for biomedical applications. Cellulose Chemistry and Technology 57 (12): 107116. https://doi.org/10.35812/CelluloseChemTechnol.2023.57.11

Carter JG (1990). Evolutionary significance of shell microstructure in the *Palaeotaxodonta, Pteriomorphia* and *Isofilibranchia* (Bivalvia: Mollusca). In: Carter JG (editor). Skeletal Biomineralization: Patterns. Processes and Evolutionary Trends 1: 35-296. https://doi.org/10.1007/978-1-4899-5740-5_10

Carter JG, Harries PJ, Malchus N, Sartori AF, Anderson LC et al. (2012). Illustrated glossary of the Bivalvia. Treatise Online 48: Part N (Bivalvia), Revised Part N 1 (31): 209-218.

Chakraborty A, Parveen S, Chanda DK, Aditya G (2020). Insight into the structure, composition and hardness of a biological material: the shell of freshwater mussels. The Royal Society of Chemistry Advances 10: 29543-29554. https://doi.org/10.1039/d0ra04271d

Dauphin Y, Luquet G, Salome M, Bellot-Gurlet L, Cuif JP (2018). Structure and composition of *Unio pictorum* shell: arguments for the diversity of the nacroprismatic arrangement in molluscs. Journal of Microscopy 270 (2): 156-169. https://doi.org/10.1111/jmi.12669

Delali H, Merouani DR, Aguedal H, Belhakem M, Iddou A et al. (2019). Valorisation of waste mussel shells as biosorbent for an Azo dye elimination. Key Engineering Materials 800: 187-192. https://doi.org/10.4028/www.scientific.net/KEM.800.187

El-Bassyouni GT, Eldera SS, Kenawy SH, Hamzawy EM (2020). Hydroxyapatite nanoparticles derived from mussel shells for in vitro cytotoxicity test and cell viability. Heliyon 6 (6): e04085. https://doi.org/10.1016/j.heliyon.2020.e04085.

Froufe E, Pri e V, Faria J, Ghamizi M, Gonçalves DV et al. (2016). Phylogeny, phylogeography, and evolution in the Mediterranean region: news from a freshwater mussel (*Potomida, Unionida*). Molecular Phylogenetics and Evolution 100: 322-332. https://doi.org/10.1016/j.ympev.2016.04.030.

González-Chang M, Boyer S, Creasy GL, Lefort MC, Wratten SD (2017). Mussel shell mulch can increase vineyard sustainability by changing scarab pest behaviour. Agronomy for Sustainable Development 37: 1-9. https://doi.org/10.1007/s13593-017-0450-x

Haag WR (2012). North American Freshwater Mussels: Natural History, Ecology, and Conservation. Cambridge University Press, New York 538 p.

Hamester MRR, Balzer PS, Becke, D (2012). Characterization of calcium carbonate obtained from oyster and mussel shells and incorporation in polypropylene. Materials Research 15 (2): 204-208. https://doi.org/10.1590/S1516-14392012005000014

Hedegaard C (1990). Shell Structures of the Recent Archaeogastropoda. PhD Thesis, University of Aarhus, Aarhus, Denmark.

Hedegaard C (1997). Shell structures of the recent Vetigastropoda. Journal of Molluscan Studies 63: 369-377. https://doi.org/10.1093/mollus/63.3.369

Hossain A, Aditya G (2013). Cadmium biosorption potential of shell dust of the fresh water invasive snail Physa acuta. Journal of Environmental Chemical Engineering 1 (3): 574-580. https://doi.org/10.1016/j.jece.2013.06.030

Hossain MM, Kabir MSH, Chowdhury TA, Hasanat A, Chakrabarty N (2015). Anthelmintic effects of different extracts of *Hopea odorata* leaves on *Tubifex tubifex* worm using in vitro method and their condensed tannin content. Journal of Research in Pharmacy 8 (3): 1-7. https://doi.org/10.9734/BJPR/2015/19064

Ismail R, Fitriyana DF, Santosa YI, NugrohoS, Hakim AJ et al. (2021). The potential use of green mussel (*Perna viridis*) shells for synthetic calcium carbonate polymorphs in biomaterials. Journal of Crystal Growth 572: 126282. https://doi.org/10.1016/j.jcrysgro.2021.126282

Jackson AP, Vincent JFV, Turner RM (1988). The mechanical design of nacre. Proceedings of the Royal Society B: Biological Sciences 234: 415-440. https://doi.org/10.1098/rspb.1988.0056

Jang SY, Jeong YJ, Kwon TK, Seo JH (2010). Effects of water-soluble calcium supplements made from eggshells and oyster shells on the calcium metabolism of growing rats. Journal of Food Science and Nutrition 15 (1): 78-82. https://doi.org/10.3746/jfn.2010.15.1.078.

Kucharczyk K, Rybka JD, Hilgendorff M, Krupinski M, Slachcinski M et al. (2019). Composite spheres made of bioengineered spider silk and iron oxide nanoparticles for theranostics applications. PloS One 14 (7): e0219790. https://doi.org/10.1371/journal.pone.0219790

Latire T, Legendre F, Bouyoucef M, Marin F, Carreiras F et al. (2017). Shell extracts of the edible mussel and oyster induce an enhancement of the catabolic pathway of human skin, in vitro. Cytotechnology 69 (5): 815-829. https://doi.org/10.1007/s10616-017-0096-1.

Lee YH, Islam SMA, Hong SJ, Cho KM, Math RK et al. (2010). Composted oyster shell as lime fertilizer is more effective than fresh oyster shell. Bioscience, Biotechnology, and Biochemistry 74 (8): 1517-1521. https://doi.org/10.1271/bbb.90642

Lowenstam HA, Weiner S (1989). On Biomineralization, 324, New York: Oxford University Press. Academic.

Lopes-Lima M, Rocha A, Gonçalve, F Andrade J, Machado J (2010). Microstructural characterization of inner shell layers in the freshwater bivalve *Anodonta cygnea,* Journal of Shellfish Research 29 (4): 969-973. https://doi.org/10.2983/035.029.0431

Lopes-Lima M, Gürlek ME, Kebapçı Ü, Şereflişan H, Yanık T et al. (2021). Diversity, biogeography, evolutionary relationships, and conservation of Eastern Mediterranean freshwater mussels (Bivalvia: Unionidae). Molecular Phylogenetics and Evolution 163: **107261.** https://doi.org/10.1016/j.ympev.2021.107261

Machado J, Reis ML, Coimbra J, Sá C (1991). Studies on chitin and calcification in the inner layers of the shell of *Anodonta cygnea*. Journal of Comparative Physiology A 161: 413-418. https://doi.org/10.1007/BF00260802

Marie B, Zanella-Cléon I, Le Roy N, Becchi M, Luquet G et al. (2010). Proteomic analysis of the acid-soluble nacre matrix of the bivalve unio pictorum: detection of novel carbonic anhydrase and putative protease inhibitor proteins. Chemical Biology Chemistry Europe 11 (15): 2138-2147. https://doi.org/10.1002/cbic.201000276

Marie B, Le Roy N, Zanella-Cléon I, Becchi M, Marin F (2011). Molecular evolution of mollusc shell proteins: Insights from proteomic analysis of the edible mussel Mytilus. Journal of Molecular Evolution 72: 531-546. https://doi.org/10.1007/s00239-011-9451-6

Marie B, Arivalagan J, Mathéron L, Bolbach G, Berland S et al. (2017). Deep conservation of bivalve nacre proteins highlighted by shell matrix proteomics of the Unionoida Elliptio complanata and Villosa lienosa. Journal of the Royal Society Interface 14 (126): 20160846. https://doi.org/10.1098/rsif.2016.0846

Marin F, Le Roy N, Marie B (2012). The formation and mineralization of mollusk shell. Frontiers in Bioscience-Scholar 4 (3): 1099-1125. https://doi.org/10.2741/S321

Meyers MA, Lin AYM, Chen PY, Muyco J (2008). Mechanical strength of abalone nacre: role of the soft organic layer. Journal of the Mechanical Behavior of Biomedical Materials 1 (1): 76-85. https://doi.org/10.1016/j.jmbbm.2007.03.001.

Moura G, Vilarinho L, Guedes R, Machado J (2000). The action of some heavy metals on the calcification process of *Anodonta cygnea* (Unionidae): nacre morphology and composition changes. Haliotis 29: 43-53. https://doi.org/10.1139/z11-129

Öksüz KE, Özkaya NK, İnan ZDŞ, Özer A (2021). Novel natural spider silk embedded electrospun nanofiber mats for wound healing. Materials Today Communications 26: 101942. https://doi.org/10.1016/j.mtcomm.2020.101942

Patil PP, Meshram JV, Bohara RA, Nanaware SG, Pawar SH (2018). ZnO nanoparticle embedded silk fibroin–polyvinyl alcohol composite film: A potential dressing material for infected wounds. New Journal of Chemistry 42 (17): 14620-14629. https://doi.org/10.1039/c8nj01675e

Shen Y, Zhu J, Zhang H, Zhao F (2006). In vitro osteogenetic activity of pearl. Biomaterials 27 (2): 281-287. https://doi.org/10.1016/j.biomaterials.2005.05.088

Singh S, Dod, J, Volkers P, Hethershaw E, Philippou H et al. (2019). Structure functional insights into calcium binding during the activation of coagulation factor XIII A. Scientific Reports 9 (1): 11324. https://doi.org/10.1038/s41598-019-47815-z

Sudo S, Fujikawa T, Nagakura T, Ohkubo T, Sakaguchi K et al. (1997). Structures of mollusc shell framework proteins. Nature 387 (6633): 563-564. https://doi.org/10.1038/42391

Şereflişan HO (2003). Gölbaşı Gölü (Hatay)'nde Bulunan Unio terminalis delicatus'un Üreme Biyolojisi ve Yetiştiricilik Potansiyelinin Araştırılması. Doktora Tezi. Çukurova Üniversitesi - 1319. Adana, Turkey.

Tomilova AA, Lyubas AA, Kondakov AV, Konopleva ES, Vikhrev IV et al. (2020). An endemic freshwater mussel species from the Orontes River basin in Turkey and Syria represents duck mussel's intraspecific lineage: Implications for conservation. Limnologica 84 (2): 125811. https://doi.org/10.1016/j.limno.2020.125811

Wang S, Castro R, An X, Song C, Luo Y et al. (2012). Electrospun laponite-doped poly (lactic-co-glycolic acid) nanofibers for osteogenic differentiation of human mesenchymal stem cells. Journal of Materials Chemistry 22 (44): 23357-23367. https://doi.org/10.1039/c2jm34249a

Yang X, Fan L, Ma L, Wang Y, Lin S et al. (2017). Green electrospun Manuka honey/silk fibroin fibrous matrices as potential wound dressing. Materials & Design 119: 76-84. https://doi.org/10.1016/j.matdes.2017.01.023

Yao Z, Xia M, Li H, Chen T, Ye Y et al. (2014). Bivalve shell: not an abundant useless waste but a functional and versatile biomaterial. Critical Reviews in Environmental Science and Technology 44 (22): 2502-2530. https://doi.org/10.1080/10643389.2013.829763

Zhang H, Wu X, Quan L, Ao Q (2022). Characteristics of marine biomaterials and their applications in biomedicine. Marine Drugs 20 (6): 372. https://doi.org/.3390/md20060372

Zhao Y, Sun X, Zhang G, Trewyn BG, Slowing II et al. (2011). Interaction of mesoporous silica nanoparticles with human red blood cell membranes: size and surface effects. American Chemical Society Nano 5 (2): 1366-1375. https://doi.org/10.1021 /Nn103077k